Polymer 51 (2010) 868–876

Contents lists available at ScienceDirect

Polymer

journal homepage: www.elsevier.com/locate/polymer

Polyvinyl alcohol–collagen–hydroxyapatite biocomposite nanofibrous scaffold: Mimicking the key features of natural bone at the nanoscale level

Ashraf Sh. Asran [a,b,*], S. Henning [a], Goerg H. Michler [a]

[a] Institute of Physics, Martin-Luther-University Halle-Wittenberg, D-06099 Halle/S., Germany
[b] National Research Centre, El Buhoth St., 12311 Cairo, Egypt

ARTICLE INFO

Article history:
Received 16 July 2009
Received in revised form
8 November 2009
Accepted 18 December 2009
Available online 11 January 2010

Keywords:
Bone
Electrospinning
Biocomposite nanofibers

ABSTRACT

Polyvinyl alcohol (PVA) nanofibers, PVA/Type I Collagen (Col) and their composites with hydroxyapatite nanoparticles (nano-HAp) were prepared by electrospinning techniques. The composite nanofibrous membranes were subjected to detailed analysis. Morphological investigations show that the generated nanofibers (NFs) have uniform morphology with an average diameter of ~160 nm for pure PVA, ~176 nm for PVA/n-HAp, ~245 nm for PVA/Col and ~320 nm for PVA/Col/n-HAp. It is of interest to observe that large numbers of HAp nanorods are preferentially oriented parallel to the longitudinal direction of the electrospun PVA and/or PVA/Col NFs. FTIR and thermal analysis demonstrated that there was strong intermolecular hydrogen bonding between the molecules of PVA/Col/n-HAp. Furthermore, the obtained PVA/Col/nHAp NFs scaffold (7 cm × 11 cm) has a porous structure with adjustable pore size and shape. The pore size is in the range of 650 μm with a porosity of 49.5%. On the other hand, mechanical characterizations revealed that the incorporating of 5 wt% n-HAp into the matrix of PVA/Col nanofibers could significantly improve the rigidity of the resultant biocomposite nanofibrous scaffold. These results strongly suggest a huge potential of the prepared scaffold for bone tissue engineering.

1. Introduction

Natural bone is a biocomposite material composed of nano-hybrid organic–inorganic components. The organic matrix is mainly Type I Collagen (Col) which provides bone its flexibility and resilience, the inorganic phase composed of mineral hydroxyapatite (HAp) which is responsible for the stiffness and strength of bone. The organic–inorganic constituents combine together to provide a mechanical and supportive role in the body [1]. Large bone fracture, defects, loss, infections and tumor resections are serious problems for bone surgery [2]. One strategy for dealing with serious bone damage is to develop tissue engineered bone substitutes [3]. It has been a long-term goal for biomaterial scientists to fabricate bone graft materials that can mimic the structural, mechanical, and biological behavior of natural bone [4]. Recently, mimicking the architecture of an extracellular matrix (ECM) is becoming one of the major challenges for biomaterials scientists [5]. In our previous work, we have fabricated biocompatible and biodegradable PVA/HAp nanocomposite nanofibers (NCNFs) in order to mimic mineralized hard tissues for bone and dentin replacement [6].

Col and HAp have potential in mimicking natural ECM and replacing diseased skeletal bones [7]. Furthermore, the combination of both a ceramic and a polymer within one material results in composites having the ductility of a polymer and the bioactivity of the calcium phosphate phase. Recently, studies on three-dimensional scaffold materials have become a key element of bone tissue engineering [8]. It has become a rapidly expanding research area since it offers a new and promising approach for bone repair and regeneration of fractured or diseased bones. Kikuchi et al. synthesized HAp and Col composite which could be applied for better bioactive bone graft materials [9].

Poly(vinyl alcohol) (PVA) has gained popularity as a scaffold supporting material for tissue engineering applications. It endows mechanical stability and flexibility to the conventional scaffolds made of natural polymers [10]. In addition, PVA hydrogels have been used in a number of biomedical applications including soft contact lenses [11], cartilage implants [12], drug-delivery matrices [13], temporary skin covers or burn dressings [14] and artificial organs [15]. This is because of their inherent non-toxicity, non-carcinogenicity, good biocompatibility, and desirable physical

* Corresponding author. Institute of Physics, Martin-Luther-University Halle-Wittenberg, D-06099 Halle/S., Germany. Tel: +49 345 55 25405; fax: +49 345 55 27149.
E-mail address: ashraf.abdel-sayed@physik.uni-halle.de (A.Sh. Asran).

0032-3861/$ – see front matter © 2010 Elsevier Ltd. All rights reserved.
doi:10.1016/j.polymer.2009.12.046

properties such as rubbery or elastic nature and high degree of swelling in aqueous solutions [16]. Furthermore, it has been selected as the polymer additive to produce electrospun nanofibrous mats because of its good fibers forming, biocompatibility, and chemical resistance properties [17].

Electrospinning is a novel process for forming superfine fibers with diameters ranging from 10 μm down to 10 nm by forcing a polymer solution (or polymer melt) with an electric field through a spinneret [18,19]. It has been approximated that NFs with a diameter of 100 nm have a ratio of geometrical surface area to mass of 100 m^2/g [20]. Recently, electrospun fibers have attracted great attention due to their potential applications in many fields especially in biomedical uses. The electrospun micro and/or nanofibers can be used as scaffolds for engineering tissues such as cartilages [21,22], bone [23,24], arterial blood vessels [25], heart [26], nerves [27], wound healing [28,29], vascular grafts [30], etc. In the past, several different electrospun NCNFs had been devised and explored for potential bone regeneration applications [31,32]. The main objective of our study is to design a novel biodegradable NCNFs scaffold consisting of PVA/Col with unidirectional aligned nano hydroxyapatite to mimic the nano structure of human bone tissue.

2. Experimental

2.1. Materials

Poly(vinyl alcohol) (PVA), average molecular weight (M_w) 85,000–124,000 g/mol, 87–89% hydrolyzed was purchased from Sigma–Aldrich and used without further treatment or purification. Rat tail Type I Col (6.3 mg/ml dissolved in 1 M acetic acid) was kindly donated by Faculty of Medicine, University of Halle-Wittenberg. The hydroxyapatite (HAp) nanoparticles were of commercial grade Ostim® from aap Implantate AG, Germany.

2.2. Preparation of spinning solutions

To obtain electrospinnable stock solutions, 15 wt% PVA was dissolved in de-ionized water (DI H_2O) and vigorously stirred with a magnetic stir bar at 80 °C for 8 h, then cooled to room temperature and stirred for 4 h at room temperature to ensure homogeneity. This stock solution was used to prepare all samples for electrospinning. Type I Col, extracted from rat tail tendon (6.3 mg/ml of 1 M acetic acid) has been used as a solution to dilute the 15 wt% PVA with a weight ratio of Col:PVA is (55:45), to get 7 wt% final solution. This solution stirred for 2 h at temperature below 25 °C to avoid the Col denaturation. HAp nanorods suspended in water (35%) has been added to PVA/Col solution (5 wt% and 10% based on PVA weight) for the preparation of PVA/Col/n-HAp biocomposite.

2.3. Electrospinning of the scaffold

The polymer solution was filled in a 1 ml syringe equiped with a blunt steel needle of 0.8 mm inner diameter. A round steel plate covered with aluminium foil was placed 15 cm away from the needle tip as counter electrode. Electrospinning was carried out at room temperature in a vertical spinning configuration, using applied voltages in the range from 3 to 20 kV, driven by a high voltage power supply (HEINZINGER PNC, Germany) with a flow rate of 100 μl/h. For morphological investigations, a glass plate was placed over the counter electrode as collecting substrate. The electrospun fibres were collected either directly on the aluminium foil or on grounded stainless steel network to obtain web scaffold.

3. Characterization

3.1. Electron microscopy

Samples for electron microscopy were prepared by direct electrospinning of PVA, PVA/Col, PVA/n-HAp and PVA/Col/n-HAp on the slide glasses and followed by Au sputtering to ~20 nm thickness for better conductivity during imaging. The size and morphology of the electrospun fibers were investigated by scanning electron microscopy (SEM) (JEOL JSM 6300). Average fiber diameters and their size distributions were determined by measuring over 200 fibers selected randomly from the SEM images using image analysis software (AnalySIS, Soft Imaging System Co., Germany). The morphology and particle size of the as-received HAp were investigated by conventional transmission electron microscopy (TEM) (JEOL 200CX operated at 200 kV). For characterization of HAp nanoparticles and their spatial dispersion within the electrospun fibers by TEM, samples were prepared by directly depositing NFs onto Cu-grids 3 mm diameter covered with an ultrathin carbon layer. The scaffold porosity has been measured from the SEM images using analysis software (Image J, National Institute of Health, USA), according to the method of Ghasemi-Mobarakeh et al. [33].

3.2. Differential scanning calorimetry (DSC) and thermo gravimetric analysis (TGA)

Differential Scanning Calorimetry (DSC) measurements have been performed using NETZSCH DSC 204 with TASC 414/4 controller under nitrogen as purge gas. About 5 mg of sample was heat-treated from 25 to 250 °C for 2 min in order to eliminate any thermal history. Then the sample was cooled at a rate 10 °C/min to 25 °C for complete crystallization of the matrix.

The heat evolved during non-isothermal crystallization was recorded as a function of time. Then the specimens were heated again to 250 °C without prior cooling to obtain the DSC endotherms at a rate of 10 °C/min. The melting temperatures were determined from the maxima of the fusion peaks. The degree of relative crystallinity, X_c was estimated from the endothermic area by the following Equation (1):

$$X_c = \Delta H_f / \Delta H_f^o \quad (1)$$

where ΔH_f is the measured enthalpy of fusion from DSC thermograms and ΔH_f^o is the enthalpy of fusion for 100% crystalline PVA ($\Delta H_m = 138.6$ J/g from literature) [34].

Thermogravimetric Analysis (TGA) was performed using NETZSCH TG 209C. About 5 mg of sample was heat-treated from room temperature to 750 °C at a heating rate of 20 °C/min under a nitrogen flow. All the graphs were plotted for temperature °C (*X*-axis) against the heat flow, mW (*Y*-axis).

3.3. Fourier transform infrared spectroscopy (FTIR)

FTIR spectra of the electrospun NFs and NCNFs were obtained using FTIR Spectrometer S2000, Perkin–Elmer equipped with a fixed 100 μm diameter aperture. A mercury–cadmium–telluride (MCT) detector was used to analyse the absorbance in the wave number range of 500–4000 cm^{-1} with a resolution of 2 cm^{-1}.

3.4. Mechanical characterization

Mechanical properties of electrospun nanofibrous scaffolds were measured using Dia-Stron MTT 675 miniature tensile tester (Dia-Stron Ltd. Andover, UK) at 25 °C, using 10 N load cell under a constant tensile deformation rate of 10 mm min^{-1}. All samples

were cut into rectangle shapes with dimensions of 20 mm × 5 mm. The thicknesses of the samples were measured individually using Dia-Stron universal control unit (UV1000). At least seven samples were tested for each type of electrospun mats.

4. Results and discussion

4.1. Morphology of HAp nanoparticles and the electrospun NCNFs

Fig. 1 shows a TEM micrograph of HAp nanoparticles, in which the morphology of the individual HAp nanoparticles was clearly revealed to be rod-like shape. The image indicated that HAp consisted of well defined crystalline rods having a width of 10–30 nm and lengths of 20–120 nm (see Fig. 2). Most striking feature obtained from TEM investigation was that all HAp nanorods exhibited nano porous morphology on the surface, which might be useful for cell anchorage sites, providing interface to respond to physiological and biological changes and to remodel the ECM in order to integrate with the surrounding native tissue.

The morphology of electrospun pure PVA NFs is shown in Fig. 3. The as-spun PVA NFs have a uniform structure without any sign of beads formation. In addition, the electrospun nanocomposite PVA/n-HAp fibers (Fig. 4) have a morphology identical to those from pure PVA NFs. A minor increase in the average fiber size occurred by addition of HAp nanorods. Here, the average size diameter of the NCNFs shifts from ~160 nm to ~176 nm (Fig. 5). Nevertheless, the majority of diameter in both cases was in the range of 100–250 nm. The typical internal morphology of the electrospun PVA containing n-HAp revealed that the HAp nanoparticles are well distributed within the electrospun fibers, and it is of interest that a large number of HAp nanoparticles were preferentially oriented parallel to the longitudinal direction of the electrospun PVA (see Fig. 4).

PVA/Col solutions with and without n-HAp have been electrospun at the same conditions as described above. It is shown in Fig. 6 that PVA/Col NFs morphology is unchanged compared with previous PVA and PVA/HAp NCNFs, only the average fiber diameters shifted to ~245 nm. When loading of 5%, n-HAp in PVA/Col NFs, uniform nanocomposite nanofibers could be produced. The obtained PVA/Col/n-HAp have the same homogeneity as the previous NFs without any beads formation, see Fig. 7(a). An increment of their average size diameters occurred, the average size diameter increased to ~320 nm by addition of 5 wt% n-HAp and the majority of diameter in both cases was in the range of 100–530 nm. In literature, the organic matrix fibers in the natural bone tissues have diameters in the range from 100 to 450 nm [35].

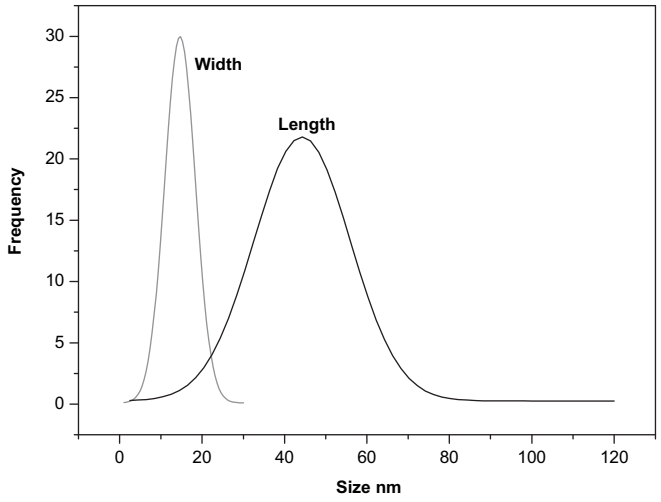

Fig. 2. Size distribution of n-HAp nanorods.

Fig. 7(b) shows the back-scattered electron image of uniaxially aligned electrospun PVA/Col/n-HAp. It is shown that addition of 10 wt% n-HAp (based on weight of PVA) exhibits some agglomeration of n-HAp along the fibers axis, and the size of the agglomerated n-HAp are in the range of 350–520 nm. However, the majority of n-HAp particles are arranged in the fiber direction. This nanoscale orientation resembles the orientation of HAp crystals in the mineralized ECM and Col NFs of natural bone fibril [36]. Furthermore, the aligned NFs represent an effective approach to control cell orientation and migration in tissue engineering [37]. Fig. 8 shows the final electrospun PVA/Col/n-HAp NCNFs web scaffold (7 cm × 11 cm). The scaffold has a porous structure with a controllable pore size and shape. Furthermore, the pores size is in the range of 650 μm with porosity of 49.5%. Such structure of this scaffold can be helpful for building 3D structure for tissue engineering applications [38].

4.2. FTIR measurements

FTIR spectroscopy was carried out to elucidate the presence of Col and HAp in the blended nanocomposite and to analyse any complex structural changes that might have occurred due to the blending, also to analyse the interaction (hydrogen bonding) between Col, HAp and PVA in the final NCNFs. The representative

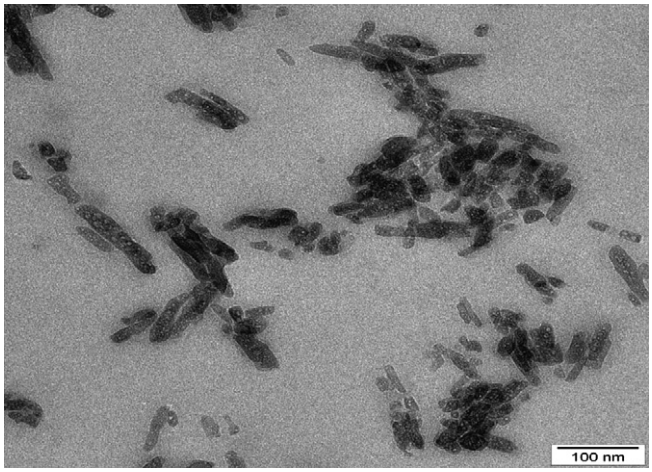

Fig. 1. TEM micrograph of HAp nanorods.

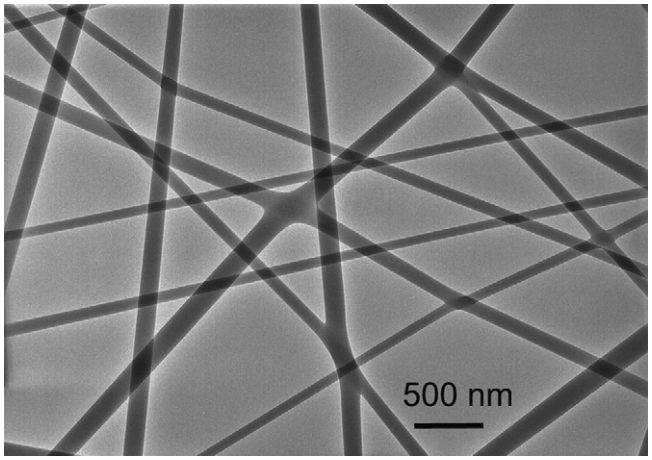

Fig. 3. TEM micrograph for electrospun PVA NFs.

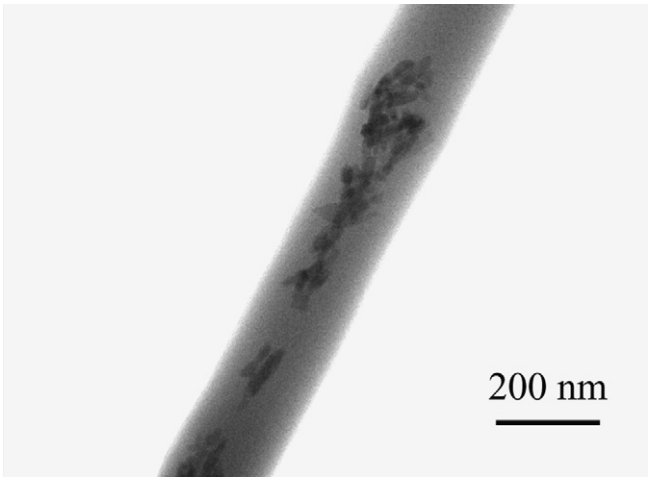

Fig. 4. TEM micrograph for electrospun PVA/n-HAp.

FTIR absorption spectra of the pure HAp nanorods, Col, Col/n-HAp, electrospun PVA, PVA/n-HAp, PVA/Col and PVA/Col/n-HAp is shown in Figs. 9 and 10 and summarized in Table 1.

The results indicate that the incorporation of n-HAp into PVA nanofibers causes a shift of the predominant broad absorption band associated with the OH stretching of PVA from 3278–3296 cm^{-1}. This result suggests that the hydrogen bonding became stronger in case of electrospun PVA/n-HAp NC than pure PVA or PVA fibers due to the increase in the number of OH groups by addition of HAp. In addition, the major absorption band of PO_4^{-3} stretching which appears at 1019 cm^{-1} in HAp's spectrum, moved to 1033 cm^{-1}. This shift might be attributed to the interactions between PVA molecules and n-HAp particles. Furthermore, the overall PVA crystallinity decreased by loading of n-HAp within the electrospun fibers, which was clearly evidenced by weakening of the crystalline band at 1143 cm^{-1}.

It is of interest to note here that the absorption bands associated with H_2O molecules distinctly appeared at 3576 cm^{-1} and 1639 cm^{-1} in the spectrum of n-HAp. The higher peak at 3576 cm^{-1} was completely missing in the electrospun fibers of PVA/n-HAp NCNFs, while the peak at 1639 cm^{-1} still exists in the spectrum in spite of a large extent of reduction in its intensity.

In conjunction with the TGA results we confirmed that the former band at 3576 cm^{-1} was identified with the loosely physisorbed water at the surface of HAp nanorods, whereas the latter arose from the chemisorbed molecular water within the HAp lattice.

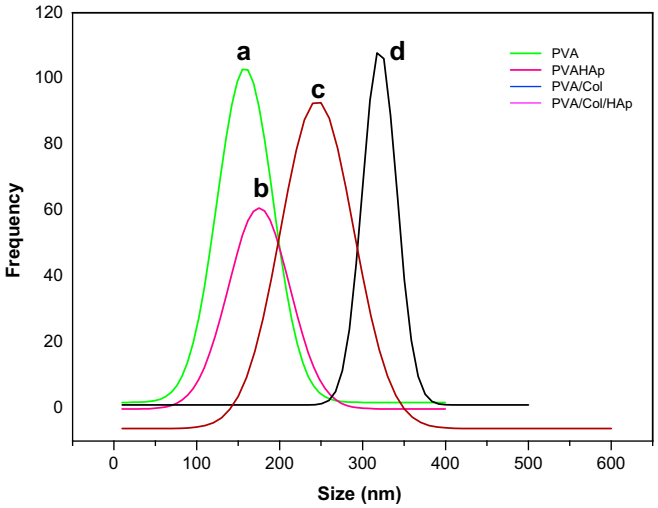

Fig. 5. (a) diameter distribution for electrospun PVA, (b) PVA/n-HAp, (c) PVA/Col and (d) PVA/Col/n-HAp.

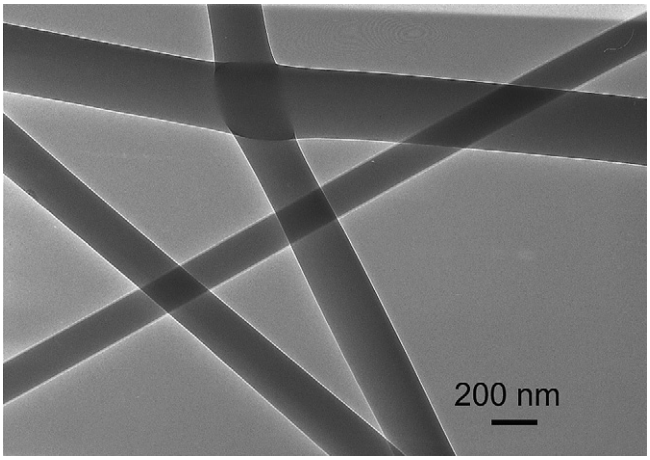

Fig. 6. TEM micrograph for electrospun PVA/Col.

The characteristic peaks of Col (Fig. 10), appears at 3312 cm^{-1} (amide A, N–H stretching and O–H stretching), 3078 cm^{-1} (amide B, C–H stretching), 1654 cm^{-1} (amide I, C=O stretching), 1552 cm^{-1}

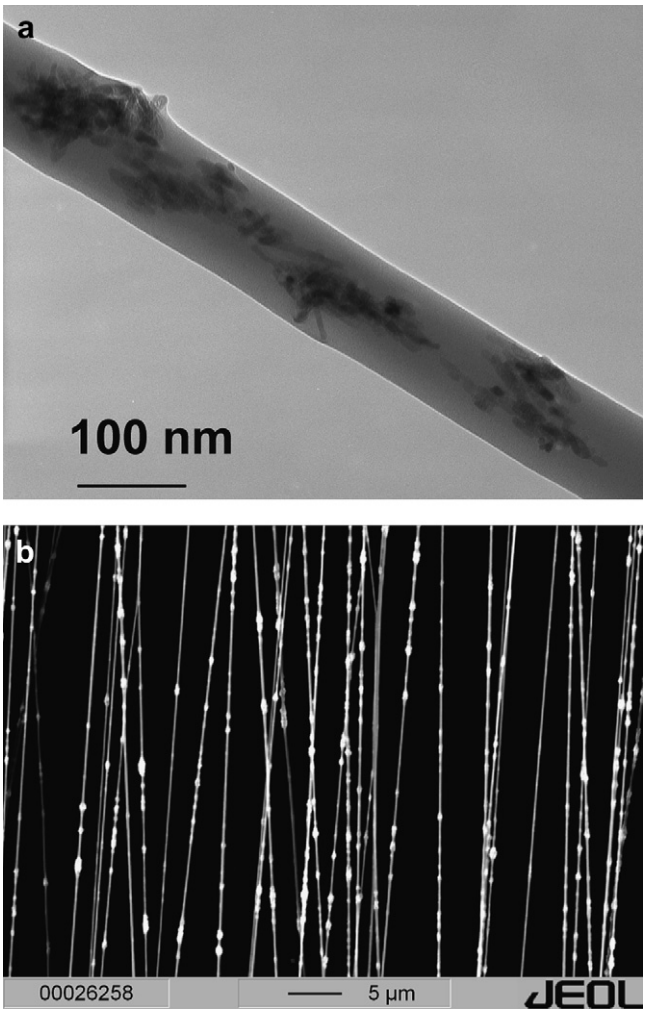

Fig. 7. (a) TEM micrograph for electrospun PVA/Col/n-HAp. (b) Back scattering SEM micrograph for aligned electrospun PVA/Col/n-HAp.

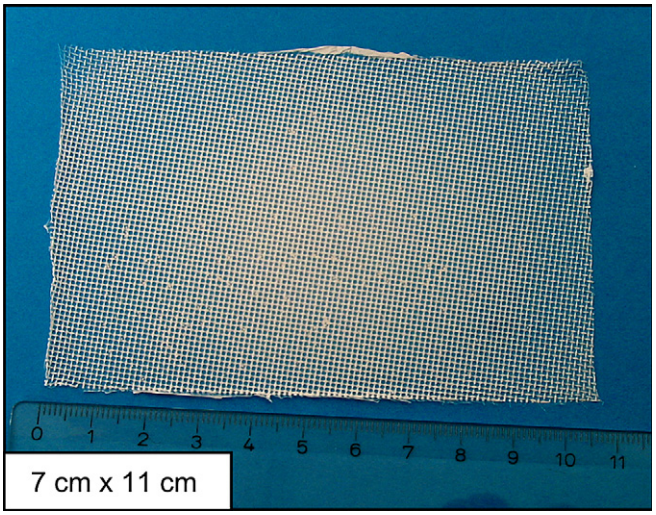

Fig. 8. Photograph of PVA/Col/n-HAp biocomposite nanofibrous scaffold.

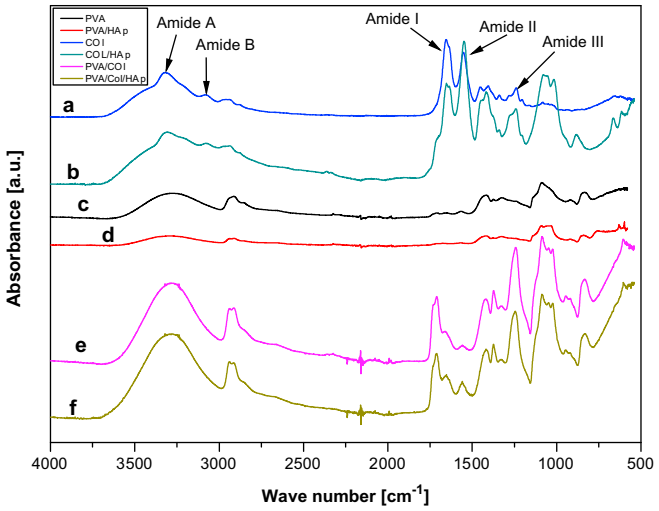

Fig. 10. (a) FTIR spectra for Col, (b) Col/n-HAp, (c) PVA, (d) PVA/n-HAp, (e) PVA/Col and (f) PVA/Col/n-HAp NCNFs.

(amide II, N–H bending and C–N stretching) and 1240 cm^{-1} (amide III, CN stretching and N–H bending) [39–41]. PVA/Col NFs spectrum shows that the amide A band shifted to lower frequencies than in collagen and the amide B band disappeared, because of amide B band was observed only for Col/PVA blend weight ratio (99:1) [42]. The spectra of PVA/Col/n-HAp NCNFs, has a small decrement for amide A compared with pure Col, accompanied by absence of amide B (due to the high amount of PVA) [42].

FTIR results demonstrated that Col can be successfully electrospun in combination with water soluble PVA and nano hydroxyapatite without any structural change of Type I Col due to electrospinning. Furthermore, there was strong intermolecular hydrogen bonding between the molecules in the electrospun PVA/Col/n-HAp biocomposite NFs due to the presence of large number of OH groups.

4.3. DSC measurements

DSC measurements have been done to investigate the thermal behaviour of the electrospun NCNFs, such as melting, crystallization and formation of crystalline structure. To characterize thermal properties of all samples in the present work, the second heating run of DSC was taken into account. The results from DSC and the characteristics observed for pure polymers and the prepared NCNFs are shown in Fig. 11 and summarized in Table 2.

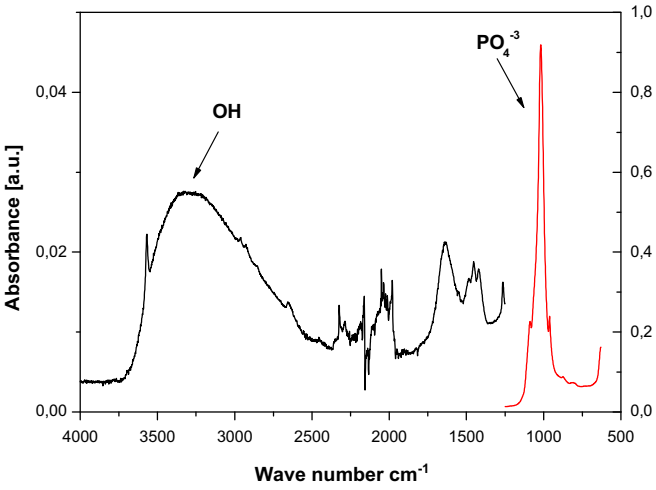

Fig. 9. FTIR spectra of pure HAp.

DSC thermogram for PVA granules in Fig. 11 shows the first endothermic peak at 41.7 °C, which is corresponding to the glass transition temperature (T_g). The glass transition temperature increased to reach 48.3 °C for the electrospun PVA NFs. The glass transition temperature of the electrospun PVA nanofibers was found to be higher than PVA granules. These results indicate that the oriented PVA chains are highly confined in the electrospun fibers. Thus, the molecular orientation limit the chain mobility and the T_g value will increase [43].

The addition of n-HAp onto PVA NFs leads to an increment of T_g (~50.3 °C). This increment could be attributed to the segmental motions of the polymer chains which were greatly constricted by the strong interactions between them through the hydrogen bonds. The second endothermic peaks (T_m) for PVA granule, PVA NFs and PVA/n-HAp NCNFs which are attributed to the melting of the crystalline phase of PVA appears at 218 °C, 219 °C and 216 °C, respectively [44].

It is observed that the melting temperature in the pure PVA granules and electrospun PVA NFs was almost the same, but the melting temperature shifted slightly to the lower value after addition of HAp nanorods in case of PVA/n-HAp NCNFs compared with others. A decrease in the enthalpy of fusion and the melting temperature suggested that the crystallinity and perfection of the crystal structure were reduced by addition of n-HAp.

The DSC for type I Col is shown in Fig. 11. A shoulder endothermic event have been observed at 30.86 °C which is corresponding to the water bonded to molecules and unfolding of the triple helical structure in diluted acetic acid [45]. Furthermore a strong endothermic event has been showed at 70.8 °C (T_m) with enthalpy of fusion (36.13 J/g), corresponded to the maximum temperature at which there was complete denaturation of the Col samples.

The DSC measurements for PVA/Col NFs with and without n-HAp (Fig. 11) show three main thermal phenomena. A shoulder peak observed at 50.7 °C, which is corresponding to glass transition of PVA. This increment also attributed to the strong interactions between the molecules through the hydrogen bonds. A broad peak at 78.2 °C corresponding to Col denaturation and strong peak at T_m 192.7 °C represents the melting of PVA. After incorporation of

Table 1
Assignments of FTIR absorption bands of pure polymers and electrospun nanofibers.

Peaks for solution (cm^{-1})				Peaks for electrospun nanofibers (cm^{-1})			Assignment
Col	HAp	Col/HAp	PVA	PVA/HAp	PVA/Col	PVA/Col/HAp	
	3567						Stretching and bending mode of H_2O (water)
3312							Amide A, N–H stretching and O–H stretching
	3316		3278	3296			Stretching of OH
3076							Amide B, C–H stretching
2949		2940	2935	2939	2923	2927	Asymmetric stretching of CH_2
			2914	2911			Symmetric stretching of CH_2
			1711	1717	1710	1713	Stretching of CO
			1657	1674			O═H, C═C
1653		1654			1657	1656	Amide I, C═O stretching
	1638						Stretching and bending mode of H_2O (water)
1552		1549			1556	1554	Amide II, N–H bending and C–N stretching
1450	1421	1413		1421		1416	Impurities (CO_2^{-3})
1404		1413	1418	1418	1422	1416	O–H, C–H bending, $\gamma(CH_2)$, δ(OH)
1341		1341	1374	1378	1372	1373	CH_2 wagging
			1326	1325	1327	1325	δ(OH) with CH wagging
1240		1240			1243	1246	Amide III, CN stretching and N–H bending
			1241	1240			C–O–C
			1143	Shoulder			Stretching of CO (crystalline sequence of PVA)
1079			1087		1083	1083	Stretching of CC and bending of OH (amorphous sequence of PVA)
	1088	1078		1092		1083	Symmetric stretching of PO_4^{-3}
	1019	1016		1033		1019	Symmetric stretching of PO_4^{-3}
	962	884		962		941	Symmetric stretching of PO_4^{-3}
			917	920	914	918	Bending of CH_2
			831	838	836	828	Rocking of CH_2
	599						PO_4^{-3} deformation vibration

n-HAp to PVA/Col NFs, the glass transition (T_g) for PVA decreased to 49 °C, the denaturation of Col occurred at 77.6 and the melting of PVA occurred at 194 °C. Sarti et al. proved that Col denaturation endotherm in PVA/Col blend shifts to higher temperature with increasing PVA content [46].

By calculating the degree of crystallinity (X_c) from the equation (1), it is found that X_c for the PVA granule is 47%, but the degree of crystallinity decreased to 44% after the electrospinning. This decrement is attributed to the strong electrostatic potential applied to a capillary which causes the jet ejection from a capillary tip with a high elongation flow rate. The polymer chains will be stretched in the electrostatic direction and the solvent will evaporate simultaneously within a very short time scale that generally leads to a lowering of the temperature (like quenching) and thereby the development of crystalline phase is considerably hindered to form perfect crystalline structure. As a consequence, the molecules in the electrospun fibers exhibit a slight decrement in the degree of crystallinity. The further decrease in crystallinity (42%) which is observed for PVA/n-HAp NCNFs can be attributed to the effect of hydroxyl groups present on the surface of HAp nanorods which serve as heterogeneous nucleation sites for PVA crystallization [47]. Furthermore, the interactions between PVA and HAp nanoparticles via hydrogen bonds induce defects in a crystalline phase in PVA. As a consequence, the decrease of the melting temperature is measured [48].

It is interesting to observe that the degree of crystallinity for PVA/Col NFs is decreased to 29.7%. This decrement is attributed to the strong hydrogen bonds occurring between Col and PVA (see Fig. 12). Col, which is a hydrogen donor, should form hydrogen bonds with the hydroxyl group of PVA even in small amounts of Col [42]. By the incorporation of HAp nanorods into PVA/Col NFs, the probability of hydrogen bonding formation increases. PVA makes hydrogen bonds between Col and HAp in the electrospun NCNFs, thus lessened the degree of crystallinity for the electrospun PVA/Col/n-HAp to 25.3%.

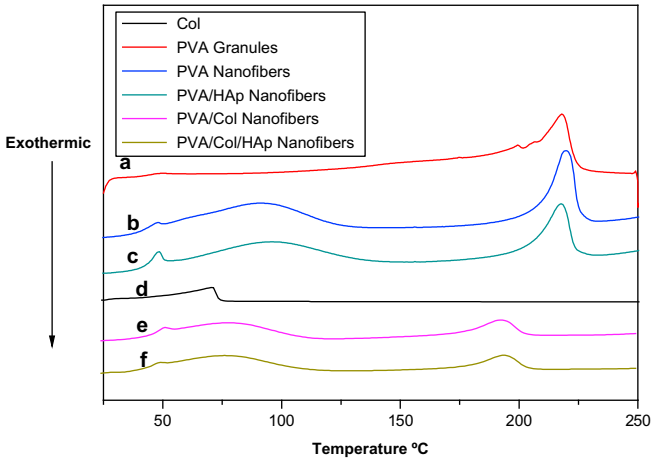

Fig. 11. (a) DSC thermograms for PVA granules,(b) electrospun PVA, (c) PVA/n-HAp, (d) Col, (e) PVA/Col and (f) PVA/Col/n-HAp.

4.4. TGA and DTGA

Fig. 13 shows typical TGA thermograms indicating the weight loss as a function of temperature for all samples. It can be observed that pure Col has an initial thermal transitional change with 63.3% mass loss in the range between 30 and 140 °C, which is attributed to the removal of water and is in accordance with a dried protein

Table 2
DSC data and the characteristics observed for the pure and electrospun polymers nanofibers.

	T_g °C	T_d °C	T_m °C	T_c °C	ΔH_m J/g	Crystallinity %
PVA granules	41.7	–	218	179	65.3	47
PVA fiber	48.3	–	219	190	61.4	44
PVA/n-HAp fiber	50.3	–	216	187	57.8	42
Col Soln	30.86	70.90	70.90	–	36.13	–
PVA/Col	50.96	78.71	192.39	93.4	41.22	29.74
PVA/Col/n-HAp	49.32	76.82	193.73	100.47	38.42	25.36

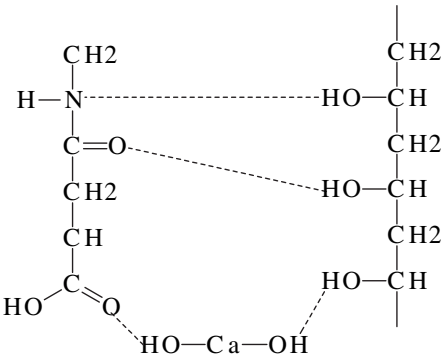

Fig. 12. Suggested hydrogen bonds between Col, n-HAp and PVA.

molecule [49]. A second transition band with ~1.8% loss weight is associated with slow decomposition of Col over a temperature range of 200–750 °C.

The TGA thermograms for electrospun PVA, PVA/n-HAp, PVA/Col and PVA/Col/n-HAp exhibited three major weight loss stages (~5 wt%) at 30–210 °C, which is refers to the weakly physisorbtion of water. The decomposition of side chain of PVA occurs in the range at 210–400 °C, and the decomposition of main chain of PVA occurs at 400–540 °C [50].

A major weight loss (~75 wt%) was observed in the range of 210–540 °C for all electrospun samples, which are correspondent to the structural decomposition of the PVA.

Fig. 14 shows the first order derivatives of TGA for all samples, refers to the temperatures at which the maximum decrease of mass occurs. It is observed that DTGA for Col has a maximum peak at ~150 °C, which is attributed to the water bound in Col. The temperature at the maximum mass loss rate for PVA NFs and PVA/n-HAp NCNFs are 308 °C and 281 °C respectively, which indicates that the decomposition of the PVA side chains was occurred readily before the main chains. The maximum mass loss rate of the electrospun PVA/n-HAp NCNFs further shifted to a lower temperature compared with that of the electrospun pure PVA. It is interesting to note here that in the first derivative of the electrospun fibers of PVA/n-HAp NCNFs exhibits a distinctive peak at 316 °C, which was not appeared in TGA curve. To identify this peak, the electrospun PVA/n-HAp NC fibers was dried in air at 85 °C for 8 h, then cooled in a desiccators and TGA was carried out again. This peak completely

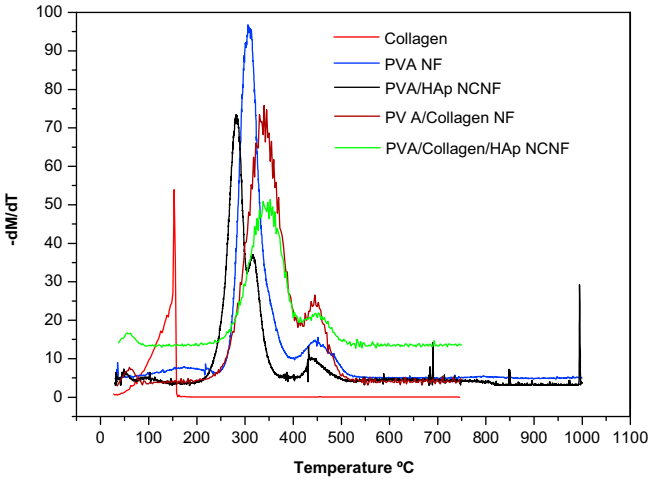

Fig. 14. (a) DTGA curves for Col, (b) electrospun PVA, (c) PVA/n-HAp, (d) PVA/Col and (e) PVA/Col/n-HAp.

disappeared in the DTGA curve of the dried electrospun PVA/n-HAp NCNFs fibers. This result clearly indicates that the peak at 316 °C arises from the loss of lattice water which may be "structural" water or water trapped within HAp nanorods. This result is consistent with the data of Rootare et al. for the chemisorbed water layer [51]. The maximum mass loss rate of the electrospun fibers of PVA/Col shifted to a higher temperature 338 °C compared with that of the electrospun pure PVA, which is attributed to the strong hydrogen bonds between Col and PVA. Furthermore, incorporation of n-HAp onto PVA/Col NFs increases the maximum mass loss rate to a higher temperature (345 °C) compared to other. This is attributed to increasing the number of hydrogen bonds between Col and n-HAp with PVA. Over ~600 °C, all TGA diagrams became flat and mainly the inorganic residue (i.e. HAp nanorods) remained. From the amounts of the residue at 800 °C, the inorganic contents of the electrospun PVA/n-HAp NCNFs was estimated of about 7.5 wt%.

4.5. Mechanical characterization

The mechanical properties of the biocomposite nanofiber scaffolds were evaluated by tensile testing; the stress–strain curves of

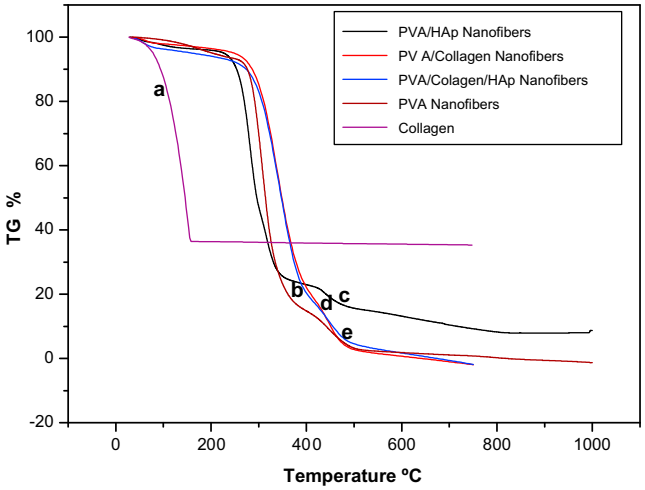

Fig. 13. (a) TGA thermograms for Col, (b) electrospun PVA, (c) PVA/n-HAp, (d) PVA/Col and (e) PVA/Col/n-HAp.

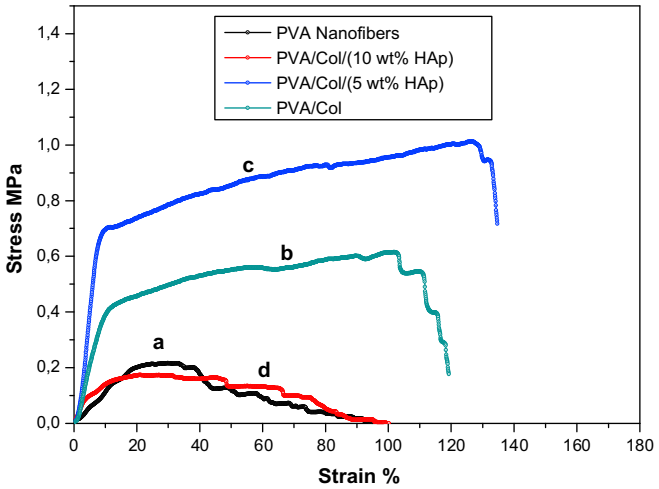

Fig. 15. (a) stress–strain for electrospun PVA, (b) PVA/Col, (c) PVA/Col/(5 wt% n-HAp) and (d) PVA/Col/(10 wt% n-HAp).

Table 3
Mechanical characteristics for the electrospun PVA, PVA/Col, PVA/Col/(5 wt% n-HAp) and PVA/Col/(10 wt% n-HAp).

Nanofibers	Elastic modulus (MPa)	Tensile strength (MPa)	Break strain (%)
PVA	2.67 ± 0.78	0.22 ± 0.09	41 ± 6.64
PVA/Col	4.97 ± 2.41	0.62 ± 0.13	109 ± 11.34
PVA/Col/(5 wt% HAp)	11.10 ± 3.38	1.03 ± 0.17	135 ± 14.25
PVA/Col/(10 wt% HAp)	3.10 ± 0.94	0.17 ± 0.05	51 ± 6.95

the samples are shown in Fig. 15 and summarized in Table 3. It is observed that the tensile strength for pure PVA NFs is (0.22 ± 0.09 MPa) and the elastic modulus is (2.67 ± 0.78 MPa). By addition of Type I Col into PVA NFs, the tensile strength increases to (0.62 ± 0.13 MPa) with an elastic modulus of (4.97 ± 2.41 MPa). The electrospun biocomposite nanofiber scaffold of PVA/Col containing 5 wt% n-HAp displays the highest tensile strength compared to the other samples, it shows a tensile strength of (1.03 ± 0.17 MPa) and the elastic modulus is (11.10 ± 3.38 MPa).

The increment of elastic modulus and tensile strength is attributed to an increase in rigidity, because n-HAp is a hard inorganic component. Furthermore, by increasing the amount of n-HAp up to 10 wt% into PVA/Col, the tensile strength decrease to (0.17 ± 0.05 MPa) and the elastic modulus decreases to (3.10 ± 0.94 MPa). This decrement is attributed to the agglomeration of HAp nanoparticles at higher concentration (10 wt%). The results obtained indicate that the loading of Col and 5 wt% n-HAp into electrospun PVA could improve the mechanical properties of the resultant NCNFs scaffold. Strong adhesion will take place between the materials by introduction of Col and n-HAp through the formation of hydrogen bonds between the materials and the rigidity of the resultant electrospun biocomposite nanofibers scaffolds will increase. Based on the mechanical property results for our biocomposite nanofiber scaffolds which are not able to attain high tensile strength, it is concluded that there is no opportunity for applications as a load-bearing bone substitute, but it can be applied as potential candidate for non load-bearing bone tissue engineering.

5. Conclusion

The results shown here provide the possibility of producing a new 3-D biocomposite NF scaffold for potential bone graft applications, which has biocompatibility and composition similar to that of bone. Microscopic photographs showed that PVA/Col/n-HAp biocomposite NFs had a similar nanostructure to bone in which the nano rod-shape HAp crystals were aligned along PVA/Col NFs. The alignment of n-HAp, Col and PVA was self-assembled by strong hydrogen bonding interaction between them. PVA/Col/n-HAp NCNFs scaffold (7 cm × 11 cm), has a porous structure with a controllable pore size and shape, the pores size are in the range of 650 μm with porosity of 49.5%. The pure electrospun PVA NFs scaffold (without n-HAp) showed a tensile strength of 0.22 ± 0.09 MPa and elastic modulus of 2.67 ± 0.78 MPa. Blending Type Col with PVA increases the tensile strength for the electrospun PVA/Col NFs to 0.62 ± 0.13 MPa and the elastic modulus to 4.97 ± 2.41 MPa. Introduction of Col and 5 wt% HAp nanoparticles increase the tensile strength of the biocomposite nanofibers scaffold to 1.03 ± 0.17 MPa and the elastic modulus to 11.10 ± 3.38 MPa. Further increase of n-HAp content up to 10 wt%, decreases the tensile strength to 0.17 ± 0.05 MPa and the elastic modulus to 3 0.10 ± 0.94 MPa. In conclusion, the most striking properties of electrospun PVA/Col/n-HAp biocomposite NF scaffold not only the composition but also mimicking the hierarchical structure of ECM and mineral organization in bone at the nanoscale level which might be open up a wide variety of future applications for higher bioactive bone graft materials especially for non load-bearing bone tissue engineering.

Acknowledgements

The authors would like to thank Dr. Ilona Schön (Faculty of Medicine, University of Halle-Wittenberg) for supporting us by providing Type I Col. We gratefully acknowledge Mr Volker Seydewitz for conducting the TEM experiments, and Dr. André Wutzler for technical assistance with FTIR measurements.

References

[1] Zhang Y, Venugopal JR, El-Turki A, Ramakrishna S, Su B, Lim CT. Biomaterials 2008;29:4314–22.
[2] Ahlborg HG, Johnell O, Turner CH, Karlsson MK. N Eng J Med 2003;349:327–34.
[3] Hing KA. Int J Appl Ceram Technol 2005;2:184–99.
[4] Rose FRAJ, Oreffo ROC. Biochem Biophys Res Commun 2002;292:1–7.
[5] Venugopal J, Vadgama P, Kumar TSS, Ramakrishna S. Nanotechnology 2007;18:1–8.
[6] Kim G-M, Asran ASh, Michler GH, Simon P, Kim J-S. Bioinspir Biomim 2008;3:1–12.
[7] Wahl D, Czernuszka J. Eur Cell Mater 2006;11(4):3–56.
[8] Jansen EJP, Sladek REJ, Bahar H, Yaffe A, Gijbels MJ, Kuijer R, et al. Biomaterials 2005;26:4423–31.
[9] Kikuchi M, Itoh S, Ichinose S, Shinomiya K, Tanaka J. Biomaterials 2002;22:1705–11.
[10] Nho YC, Moon SW, Lee KH, Park CW, Suh TS, Jung YJ, et al. J Ind Eng Chem 2005;11:159–64.
[11] Hyon SH, Cha WI, Ikada Y, Kita M, Ogura Y, Honda Y. J Biomater Sci Polym Ed 1994;5:397–406.
[12] Juang JH, Bonner WS, Ogawa YJ, Vacanti P, Weir GC. Transplantation 1996;61:1557–61.
[13] Thanoo BC, Sunny MC, Jayakrishnan A. J Pharm Pharmacol 1993;45:16–20.
[14] Peppas NA, Scott JE. J Control Release 1992;18:95–100.
[15] Kobayashi M, Oka M. Artif Organs 2004;28:734–8.
[16] Kobayashi M, Toguchid J, Oka M. Biomaterials 2003;24:639–47.
[17] Krumora M, Lopez D, Benarente R, Mijangos C, Perena JM. Polymer 2000;41:9265–72.
[18] Reneker D, Yarin A, Fong H, Koombhongse S. J Appl Phys 2000;87:4531–47.
[19] Hohman MM, Michael S, Gregory R, Brenner MP. Phys Fluids 2001;13:2201–20.
[20] Frenot A, Chronakis IS. Curr Opin Colloid Interface Sci 2003;8:64–75.
[21] Subramanian A, Lin H, Vu D, Larsen G. Biomed Sci Instrum 2004;40:117–22.
[22] Li WJ, Danielson KG, Alexander PG, Tuna RS. J Biomed Mater Res 2003;67A:1105–14.
[23] Tuzlakoglu K, Bolgen N, Salgado A, Gomes M. J Mater Sci Mater Med 2005;16:1099–104.
[24] Yoshimoto H, Shin YM, Terai H, Vacanti JP. Biomaterials 2003;24:2077–82.
[25] Mo XM, Xu CY, Kotaki M, Ramakrishna S. Biomaterials 2004;25:1883–90.
[26] Zong X, Bien H, Chung C, Yin L, Kim K, Fang DF, et al. Polymer Preprints 2003;44:96–7.
[27] Silva GA, Czeisler C, Niece KL, Beniash E, Harrington D, Kessler JA, et al. Science 2004;303:1352–5.
[28] Yang F, Murugan R, Wang S, Ramakrishna S. Biomaterials 2005;26:2603–10.
[29] Khil M, Cha D, Kim H, Kim I, Bhattarai N. J Biomed Mater Res B Appl Biomater 2003;67:675–9.
[30] Buttafoco L, Kolkman N, Poot A, Dijkstra P, Vermes I, Feijen J. J Control Release 2005;101:322–4.
[31] Sui G, Yang X, Mei F, Hu X, Chen G, Deng Xea. J Biomed Mater Res Part A 2007;82A:445–54.
[32] Catledge S, Clem WC, Shrikishen N, Chowdhury S, Stanishevsky A, Koopman M, et al. Biomed Mater 2007;2:142–5.
[33] Ghasemi-Mobarakeh L, Semnani D, Morshed M. J Appl Polym Sci 2007;106:2536–42.
[34] Peppas N, Merrill E. J Appl Polym Sci 1976;20:1457–65.
[35] Zhen HP, Nie J, Guo S, Sun JF, Yang DZ. Acta Polymerica Sinica 2007;6:230.
[36] Du C, Cui FZ, Zhu XD, Groot Kd. J Biomed Mater Res Part A 1999;44:407–15.
[37] Xu CY, Inai R, Kotaki M, Ramakrishna S. Biomaterials 2004;25:877–86.
[38] Venugopal JR, Zhang Y, Ramakrishna S. Artif Organs; 30:440–446.
[39] Sionkowska A, Wisniewski M, Skopinska J, Kennedy CJ, Wess TJ. Biomaterials 2004;25:795–801.
[40] Jackson M, Choo L, Watson P, Halliday W, Mantsch H. Biochim Biophys Acta 1995;1270:1–6.
[41] Renugopalakrishnan V, Chandrakasan G, Moore S, Hutson T, Berney C, Bhatnagar R. Macromolecules 1989;22:4121–4.
[42] Sionkowska A, Skopiñska J, Wisniewski M. Polym Degrad Stab 2004;83:117–25.

[43] Zonga X, Kima K, Fangb D, Rana S, Hsiaoa BS, Chu B. Polymer 2002;43: 4403–12.
[44] Buckley CP, Kovacs AJ. Structure of crystalline polymers. In: Hall IH, editor. Applied science. London: Elsevier; 1984.
[45] Persikov AV, Xu Y, Brodsky B. Protein Sci 2004;13:893–902.
[46] Sarti B, Scandola M. Biomaterials 1995;16:785–92.
[47] Nayar S, Pramanick AK, Sharma BK, Das G, Kumar BR, Sinha A. Mater Sci Mater Med 2008;19:301–4.
[48] Pramanik N, Biswas SK, Pramanik P. Int J Appl Ceram Technol 2008;5:20–8.
[49] Puett D. Biopolymers 1967;5:327–30.
[50] Chikako N, Takeo S, Toshio Y, Masataka S. Fuel 1998;77:321–6.
[51] Rootare HM, Craig RG. J Dent Res 1977;56:744–7.